Journal of Catalysis 425 (2023) 20–31

Contents lists available at ScienceDirect

Journal of Catalysis

journal homepage: www.elsevier.com/locate/jcat

Evolution of reaction mechanism in the catalytic combustion of ammonia on copper-cerium mixed oxide

Huan Liu [a,b], Yang Zhao [c], Chenhang Zhang [a,c], Zibing Wang [b], Feng Bin [a,*], Xiaolin Wei [a], Baojuan Dou [c,*]

[a] State Key Laboratory of High-Temperature Gas Dynamics, Institute of Mechanics, Chinese Academy of Sciences, Beijing 100190, PR China
[b] North China University of Science and Technology, Tangshan 063210, Hebei, PR China
[c] College of Marine and Environmental Science, Tianjin University of Science & Technology, Tianjin 30022, PR China

ARTICLE INFO

Article history:
Received 14 December 2022
Revised 31 May 2023
Accepted 2 June 2023
Available online 5 June 2023

Keywords:
Catalytic combustion
Ammonia
$CuO\text{-}CeO_2$
Reaction mechanism
High concentration

ABSTRACT

Carbon-free hydrogen-rich ammonia (NH_3) is a potential next energy generation source, where a high ignition point and high nitric oxide contents, thereby limiting further development. This study aims to investigate the mechanism evolution during the catalytic ignition process of high NH_3 concentration over copper-cerium catalyst to address the demerits of flame combustion. The phase composition, elemental valence, and active species of the copper-cerium oxide ($CuO\text{-}CeO_2$) catalyst are investigated using various characterization techniques. The results indicated that Cu species are mainly present in copper-cerium solid solutions and highly dispersed CuO clusters, providing sufficient Cu sites to adsorb NH_3 and abundant reactive lattice oxygen. The catalytic ignition triggered a kinetic transition from low-rate to high-rate steady-state. During the induction process, the predominance of the L-H mechanism is implied by the kinetic modeling and transient experiments (low-rate induced phase). Combined with IR spectroscopy and isotope ($^{18}O_2$)-transient response study, the results indicated that adsorbed NH_3 reacted with surface adsorbed oxygen, simultaneously pulling out lattice oxygen to react with adsorbed NH_3, confirming the coexistence of L-H and M−K mechanism over $CuO\text{-}CeO_2$. The L-H mechanism (^{18}O, contribution of adsorbed oxygen) plays a relatively dominant role in the induction stage, while the involvement of the M−K mechanism (^{16}O, contribution of lattice oxygen) is significantly increased in the sustained combustion stage. At both stages, NH and NH_2 served as critical species for N_2 generation (i-SCR), respectively, playing an important role in N_2 selectivity. Moreover, in the self-sustained combustion stage for $CuO\text{-}CeO_2$ (14%NH_3), the rapid gas diffusion and mass transfer facilitated the adsorption and activation of NH_3. These results are envisaged to provide theoretical support for the handling and application of high concentrations of NH_3.

1. Introduction

In the context of carbon dioxide emission reduction, a hydrogen-rich carbon-free fuel, ammonia (NH_3), has recently been considered a potential hydrogen energy carrier and storage medium. However, the high and unstable ignition points of NH_3, which usually require hydrogen or hydrocarbon fuel such as CH_4 aided combustion [1–4], and higher NO content production during ignition or combustion [2,5] limits its industrial application. The catalytic oxidation of NH_3 to produce nitrogen (N_2) and water (H_2O) has proven effective for treating low concentrations of NH_3 pollution, consequently attracting increasing interest in recent years.

Most of the studies have focused on noble metals [6–8], molecular sieves [9–11], and transition metal catalysts in the NH_3-catalyzed oxidation reaction [12–14]. Notably, the copper (Cu)-based catalysts [15–17] govern potential applications due to their excellent catalytic activity in the low-temperature region, which exceeds most of the transition metal oxides, and their high N_2 selectivity is better than noble metals. The catalytic activity and N_2 selectivity for the catalytic oxidation reaction of NH_3 are closely related to the catalyst conformation [16,17], active site [15–17], and reaction pathways [18,19]. Liang et al. [15] demonstrated that the Cu species and their dispersion significantly influence the $Cu/\gamma\text{-}Al_2O_3$ catalytic activity, and the highly dispersed CuO serves as the main NH_3 molecules adsorption site [16]. Adding Cu increases the concentration of oxygen vacancies in the $CuO\text{-}CeO_2$ catalyst, ensuring excellent activity of NH_3 oxidation and N_2 selectivity [17]. For the reaction pathways, Yuan et al. [18] reported the

* Corresponding authors.
E-mail addresses: binfeng@imech.ac.cn, bjdou@tust.edu.cn (F. Bin), binfeng@imech.ac.cn, bjdou@tust.edu.cn (B. Dou).

https://doi.org/10.1016/j.jcat.2023.06.006
0021-9517/

possible reaction pathways for the catalytic oxidation of NH_3 over V_2O_5 catalysts under anoxic or oxygen-enriched conditions, demonstrating a catalyst with efficient Ostwald reaction (NH_3 to NO conversion) and selective catalytic reduction (SCR) reaction (NH_3 to N_2 reduction) are envisaged to be possible pathways for catalytic oxidation under high O_2/NH_3 ratio conditions. Similarly, Peng et al. [19] revealed that the catalytic oxidation of NH_3 on Cu/NCNT proceeds through the i-SCR pathway, where NH_3 oxidation to NO in the initial stage proceeds to react with NH_3 and O_2 to liberate N_2 and H_2O.

The precise reaction mechanism elucidation of catalytic oxidation of NH_3 has always been challenging. The reaction mechanism of gas–solid catalytic oxidation comprises Mars-van Krevelen (M−K), Langmuir-Hinshelwood (L-H) and Eley-Rideal (E-R), where the M−K mechanism can be described as the activation of NH_3 adsorption at the active site on the catalyst surface, followed by reaction with lattice oxygen, forming defects that are replenished by absorption of gas-phase oxygen. The L-H and E-R mechanisms consist of adsorbed NH_3 and oxygen reactions, corresponding to adsorbed oxygen and gas-phase oxygen, respectively. Recently, the involvement of lattice and adsorbed oxygen have also been described in the catalytic oxidation process [16,20]. However, it did not clarify the mechanism type, i.e., M−K or L-H. In contrast, it has been reported that the reaction pathways for ceria-based catalysts in NH_3-SCR reactions can be broadly classified into two categories, i.e., L-H and E-R mechanism [21,22], and the process of NH_3 catalytic oxidation is related to SCR [23], suggesting the possibility of a relevant mechanism in the catalytic combustion process. Furthermore, the current literature on the catalytic oxidation reaction of NH_3 at low concentrations is relatively clear [24,25]; however, the catalytic combustion of NH_3 at high concentrations has yet to be reported. Most studies used IR spectroscopy, density functional theory (DFT) calculations, and other methods to analyze the whole reaction pathways. However, the reaction pathways or mechanisms of the induced and sustained combustion stages have not been elaborated in combination with the different reaction stages corresponding to the activity test, considering the temperature boundary. Besides, the key intermediate species involved in the vital reaction pathways for the generation of N_2 are not yet clearly understood at different temperatures.

The project mainly contributes to the self-sustained catalytic combustion mode for high NH_3 concentration on CuO, CeO_2 and CuO-CeO_2 catalysts prepared by the sol–gel method, aiming to reveal the mechanism at different states. The synergistic relationship of copper and cerium, the evolution of reaction paths during the transition from low temperature steady state to high temperature steady state, and the mechanisms at the induction and sustained combustion stages are investigated systematically, which is envisaged to provide a theoretical foundation for handling and application of high concentration of NH_3.

2. Experimental

2.1. Preparation of catalysts

The CuO-CeO_2 mixed oxide was prepared by sol–gel method, where the nitrates of copper and cerium as a precursors in molar ratio of 1:1 was dissolved in 500 ml ethanol at 80 °C. Subsequently, oxalic acid (0.24 mol/L) was quickly added into the nitrate solution and stirred at 80 °C to make it fully dissolved until ethanol was completely evaporated to form a gel. The gel was placed at room temperature for 48 h and then dried in a vacuum drying oven at 105 °C for 12 h. Ultimately, it was calcined in a Muffle oven at 600 °C for 4 h to get the finished product. The bulk CuO and CeO_2 catalysts were also prepared by the same procedure. The reagents used in the preparation of catalysts were analytically pure ($Cu(NO_3)_2{\cdot}3H_2O$, $Ce(NO_3)_2{\cdot}6H_2O$, $C_2H_2O_4$ and C_2H_6O) from Aladdin and Macklin in Shanghai, China, respectively.

2.2. Characterization

Nitrogen sorption was measured with a NOVA 2000 gas sorption analyzer at liquid nitrogen temperature (−196 °C). Prior to measurement, each sample was degassed under vacuum for 8 h at 300 °C. The Brunauer − Emmett − Teller (BET) method was utilized to calculate the specific surface area using adsorption data acquired at a relative pressure (P/P_0) range of 0.05–0.25. X-ray powder diffraction (XRD) patterns of each catalyst were determined on XD-3 automatic diffractometer (PERSEE) with a Cu-Kα radiation (40 kV, 200 mA, λ = 1.5418 Å). X-ray photoelectron spectroscopy (XPS) was performed on a Kratos Axis Ultra DLD spectrometer equipped with Mg-Kα radiation. Raman spectra were collected by a HORIBA LabRAM HR Evolution with a 488 nm excitation laser. The H_2-temperature programmed reduction (H_2-TPR) analysis of the catalysts was carried out by a TP5080B chemisorption analyzer, coupled with a thermal conductivity detector (TCD). Heat to 300 °C by passing Ar, pretreat for 30 min and then cool to room temperature. And then the 50 mg sample was heated from room temperature to 700 °C at 10 °C /min under the condition of 5% H_2/Ar, all of that investigated the reduction ability of samples. The NH_3-TPD-MS experiments were also carried out by the TP5080B instrument. Heated to 300 °C by passing Ar and cooled to room temperature, then 5% NH_3/Ar was adsorbed respectively at room temperature for 30 min, and then the adsorption was heated at a rate of 15 °C/min until 800 °C by Ar purging. Meanwhile, the desorption signals were monitored timely by a quadrupole mass spectrometer (Pfeiffer Prisma Plus). Transient response experiments were performed using the micro-reaction fixed-bed quartz reactor combined with the transient response platform. Transient experimental procedure: 1) pretreatment with Ar by heating to 300 °C for 30 min and then cooling to room temperature; 2) pass 5% NH_3/Ar and adsorb at room temperature for 30 min, 3) purge with Ar to 200 ℃ (the induction stage) or 300 °C (the sustained combustion stage) at 10 °C /min and keep the temperature constant until the baseline is smooth; 4) In the induction stage: instantaneously pass 8% O_2/Ar and observe the change of each gas signal; In the sustained combustion stage: a) instantaneous passage of 5% NH_3 + 8% O_2/Ar into the reactor; b) Ar purge until the gas signal is smooth; c) instantaneously pass 5% NH_3/Ar and observe the change of each gas signal. The isotope ($^{18}O_2$) experiment is the same as the first three steps of the transient experiment, and the fourth step: instantly pass 10 ml $^{18}O_2$/Ar and observe the gas signal change. In situ infrared experiments were employed to detect the detailed reaction process between NH_3 and O_2 on the catalyst surface online. It went through the processes of Ar heating pretreatment, cooling to room temperature, and feeding reaction gas to heat up to 500 °C (5% NH_3, 8% O_2, Ar balancing), with the heating rate of 10 °C /min and the total flow rate of 200 ml/min.

2.3. Catalytic activity test

The catalyst sample (200 mg, particle size 0.2–0.3 mm) was filled in a micro-fixed bed with quartz tube reactor (inner diameter 4 mm) A K-type thermocouple was located between the reactor wall and the furnace wall to control the furnace temperature, while another one was inserted into the catalyst to monitor the bed temperature. The flow rates of NH_3, O_2 and Ar were controlled by mass flow controllers, where Ar was the equilibrium gas with the total flow rate of 200 ml/min. The catalytic activity was investigated for 2.5%, 6%, 10% and 14% NH_3 concentration by temperature-

programed oxidation (TPO) method for oxidation reaction. The NH_3 and O_2 were passed through at a different equivalent ratio and the temperature of the catalyst bed was raised from room temperature to 500 °C at a heating rate of 10 °C /min. Mass spectrometry was used to monitor the amount of NH_3, O_2, Ar and other products online.

3. Results and discussion

3.1. BET, XRD, Raman and XPS analysis of catalysts

The specific surface areas of CuO, CeO_2 and CuO-CeO_2 catalysts are determined by the BET surface area, which is found to be 5.8 m^2/g, 69.5 m^2/g and 47.2 m^2/g, respectively (Table 1). The XRD patterns in Fig. 1A verified that CuO and CeO_2 are the dominant phases of the CuO-CeO_2 catalyst. The diffraction peaks appeared near 2θ = 35.5° and 38.7° for the CuO-CeO_2 and are associated with (−111) and (111) planes, respectively, in the monoclinic crystal structure [26] (JCPDS 45–0937), with the crystallite size of 75.8 and 12.7 nm respectively, which is determined by Scherrer equation. In the case of pure CeO_2, the diffraction peaks at approximately 2θ = 28.6°, 33°, 47.5°, and 56.3°, corresponding to the (111), (200), (220) and (311) planes, respectively (JCPDS 34–0394). Comparing the diffraction peaks, the peak broadening and shrinking of CuO-CeO_2 indicated the formation of Cu–O-Ce solid solution, where some Cu ions are incorporated into the CeO_2 lattice. Thus, the inconspicuous CuO phase in XRD patterns arises from uniformly distributed Cu species that might be finely dispersed as CuO_x clusters on CeO_2.

The Raman spectral analysis, as shown in Fig. 1B, shows that pure CeO_2 exhibits the main band at approximately 465 cm^{-1}, which appears to be due to the symmetric F_{2g} vibration mode of the cubic fluorite structure, while the weak band at 1102 cm^{-1} is mainly attributed to the primary A_{lg} asymmetry. The Raman analysis of CuO reveals a monoclinal copper oxide phase, with A_{lg}, B_{1g} and B_{2g} modes located at 286, 333 and 618 cm^{-1}, respectively. The comparing results show that the F_{2g} band position, which appears at 465 cm^{-1} for pure CeO_2, shifted to a lower wave number in CuO-CeO_2 due to the lattice distortion of CeO_2 induced by the addition of Cu ions and the formation of oxygen vacancies in the catalyst. The peak area ratio analysis (i.e., 597 (588) and 465 (452) cm^{-1} (A_{597}/A_{465}, A_{588}/A_{452})) revealed the semi-quantitative concentration of surface vacancies to be in the order of CuO-CeO_2 (0.39) > CeO_2 (0.08) > CuO (0.00).

The chemical states, and surface compositions of the catalysts are investigated by XPS. The binding energies of Cu $2p_{3/2}$ (Fig. 1C) appear at 933.4 eV (Cu^+) and 934.8 eV (Cu^{2+}) along with satellite lines at 945–940 eV, which indicated that the redox of Cu^{2+}/Cu^+ existed in both CuO and CuO-CeO_2 catalysts [27]. The deconvoluted spectra of the Ce 3d region can be well-fitted with eight peaks (Fig. 1D) for the bulk of the CeO_2 and CuO-CeO_2. The peaks at v (881.5 eV), v_2 (887.6 eV) and v_3 (897.5 eV) correspond to the $3d_{3/2}$ level of Ce^{4+}, while the peaks tagged as u (899.9 eV), u_2 (906.1 eV) and u_3 (915.8 eV) are assigned to the $3d_{5/2}$ of the Ce^{4+} state, respectively [28,29]. The v_1-u_1 coupling denoted the fingerprint of Ce^{3+} species, which is also conducive to forming oxygen vacancies on the catalyst surface, leading to the release/storage of oxygen between Ce^{3+} and Ce^{4+}. By integrating the peak area of Cu 2p and Ce 3d, the surface composition of copper and cerium can be obtained, as shown in Table 1. The Cu^+/Cu^{2+} is calculated by the ratio of the relative area between the Cu^+ and Cu^{2+} peaks, and similarly for Ce^{3+}/Ce^{4+}, and the results are shown in Table 1, which indicated that the ratios of Cu^+/Cu and Ce^{3+}/Ce are higher than that of CuO and CeO_2, respectively. Therefore, combined with the generation of oxygen vacancies as measured via Raman spectroscopy, the Cu^{2+} and Ce^{4+} species can be reduced to Cu^+ and Ce^{3+} at the Cu-Ce interface, and at the same time to form Cu^+-[O_v]-Ce^{3+} ([O_v] = surface oxygen vacancy).

3.2. Temperature-programmed thermal analysis

3.2.1. H_2-TPR analysis

The redox behavior of catalysts is investigated by H_2-TPR, as shown in Fig. 1 E, F and G. The weak reducibility in > 200 °C region correspond to CeO_2 due to the poor redox potential of pure CeO_2. Moreover, the peak at 184 °C (β peak) is assigned to the reduction of CuO catalyst, mainly composed of CuO_x clusters dispersed on the surface, while the peak at 215 °C (γ peak) corresponded to a reduction in the crystallization of CuO [28,29]. Similarly, the CuO-CeO_2 appeared as an asymmetric peak that can be deconvoluted as three reduction peaks, i.e., α (155 °C), β (183 °C) and γ (201 °C), which are attributed to the reduction of Cu species in the Cu–O-Ce solid solution, the dispersion of CuO_x clusters, and the crystallization of CuO, respectively [29]. The synergistic effect of copper and cerium significantly reduced the CuO-CeO_2 (β and γ peak) reduction temperature, compared to pure CeO_2 and CuO. The hydrogen (H_2) consumption calculations of three catalysts are also performed where the peak area represents the consumption, i.e., the number of species, and the peak temperature reflects the reduction difficulty. The H_2 reduction peaks of the three catalysts show the reduction of Cu^{2+}, Cu^+ and Ce^{4+}, where the Cu^{2+} reduction to Cu^+ and Cu^+ reduction to Cu is envisaged to produce one H^+ each. However, the reduction peaks of Cu^{2+} and Cu^+ are close, making the two reduction processes indistinguishable. Similarly, the reduction of Ce^{4+} to Ce^{3+} will produce an H^+, whereas the reduction of Ce^{3+} to Ce^0 is impossible at a temperature < 1000 °C. As shown in Table 1, the H_2-TPR results showed that the total amount of reducible Cu in the CuO catalyst is 44.4 mmol·g^{-1}, higher than CuO-CeO_2 (34.2 mmol·g^{-1}). Furthermore, combined with the above characterization results, the H_2 consumption of the surficial Cu species, including the $CuCeO_x$ solid solution and the high dispersion CuO_x cluster content of CuO-CeO_2 catalyst are 29 mmol·g^{-1} (14.1 mmol·g^{-1} for α peak and 14.9 mmol·g^{-1} for β peak, respectively), showing strong NH_3 adsorption and oxidation capacity. Although the surface area of CuO is one order of magnitude lower than that of CuO-CeO_2, the H_2 consumption of highly dispersed CuO_x clusters in CuO catalyst is 32.5 mmol·g^{-1} (β peak), possessing comparable abundant active Cu sites with the CuO-CeO_2. In addition, the activity tests of catalysts (to be discussed subsequently) further confirmed that the redox performance of the catalyst is dependent primarily on the reduction temperature rather than the H_2 consumption in the sequence of CuO-CeO_2 > CuO > CeO_2.

Table 1
Surface compositions, H_2 consumption and BET surface areas of catalysts.

Catalyst	Surface atomic ratio		H_2 consumption (mmol/g)				BET surface area (m^2/g)
	Cu^+/Cu	Ce^{3+}/Ce	α	β	γ	Total	
CuO	0.33	/	0	32.5	11.9	44.4	5.8
CeO_2	/	0.11	0	0	0	0	69.5
CuO-CeO_2	0.55	0.15	14.1	14.9	5.20	34.2	47.2

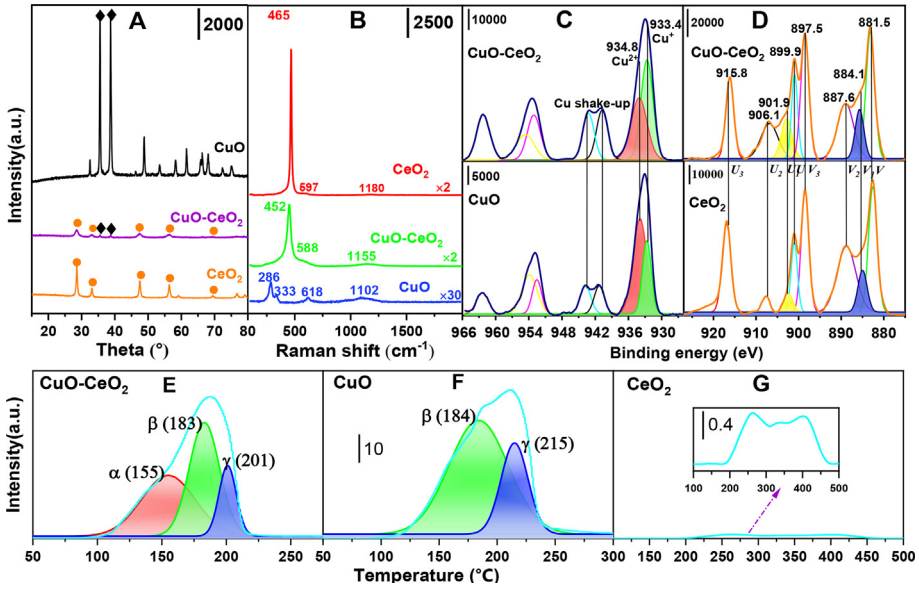

Fig. 1. XRD patterns (A), Raman spectra (B) and XPS (C, D) narrow spectra of Cu 2p and Ce 3d over the CuO, CeO_2 and CuO-CeO_2 catalysts. Reduction performance for CuO-CeO_2 (E), CuO (F) and CeO_2 (G). Blue line: original data; Smooth line: fitting line. Weight of catalyst: 50 mg; Pretreatment: 100% Ar at 550 °C for 30 min; Measurement conditions: 5% H_2/Ar (50 ml/min), heating rate10 °C/min from 50 ~ 700 °C. (For interpretation of the references to colour in this figure legend, the reader is referred to the web version of this article.)

3.2.2. NH_3-TPD-MS analysis

The adsorption-activation process and reaction mechanism of NH_3 over the catalyst are elucidated using the temperature-programmed desorption of ammonia (NH_3-TPD) technique, and the products are analyzed by mass spectrometry. As shown in Fig. 2A, the CuO-CeO_2 catalyst exhibits two NH_3 desorption peaks, where the NH_3 desorption peak at 180 °C is attributed to weak chemisorption of NH_3, while the desorption peak at 283 °C is attributed to the chemisorption NH_3 on the strong Lewis acid sites [29–31]. Moreover, the NH_3 desorption peaks for the CuO-CeO_2 catalyst cover a wide temperature range, approximately 68 ~ 398 °C, indicating adsorbed ammonia species with different thermal stabilities. Between 250 and 570 °C, the abundant reactive oxygen species on the CuO-CeO_2 surface enter oxygen vacancies (Cu^+-[O_v]- Ce^{3+}) and readily participate in the oxidation reaction. Moreover, much N_2 and NO_x are still generated on the CuO-CeO_2 catalyst after 600 °C. The lattice oxygen (O_{lat}) escape from the Cu cation and migrate to the surface, followed by a reaction with the formed ammonia species due to a concentration gradient [32].

In contrast, there is no significant NH_3 desorption for the CuO catalyst; however, the N_2 and N_2O peaks for the CuO implied that the strong oxidation capacity induced by CuO resulted in the high conversion of NH_3, which is equally prone to over-oxidation of ammonia species to NO_x which is further verified in activity experiments described in the later section. Compared with CuO-CeO_2, the CuO generates N_2 and N_2O at temperatures higher than 700 °C, indicating that the CuO also exhibited the O_{lat} mobility that might accelerate the transfer of oxygen from the bulk to the surface, which can aptly explain one of the reasons for its strong oxidation ability even under high concentration of NH_3 catalyzed oxidation. It is evident that, despite the weak redox ability of CeO_2, it has a strong NH_3 adsorption capacity, resulting in a small amount of N_2O generation. In addition, the CeO_2 generates a weak N_2 peak and a certain NO_x amount above 600 °C due to its limited O_{lat} mobility [33]. Using the Freeman-Carroll kinetic method [34], the activation energy and the reaction order in the curve's linear differential region are evaluated **(Supplementary Note 1)**. The results indicated that the activation energies for CuO-CeO_2 are lower than those of single-component CuO and CeO_2, which are 127 kJ/mol (N_2), 96 kJ/mol (NH_3), 112 kJ/mol (NH_3), respectively, indicating more potent abilities of NH_3 desorption and N_2 generation.

As discussed in earlier results, the CuO-CeO_2 catalyst shows substantial adsorption of ammonia species, mainly concentrated at the Lewis acidic sites. Considering its good oxidation ability, the surface is enriched with many intermediate HNO and NO_x species during the oxidation process, reflected in the in-situ IR results in the subsequent section. Not only the adsorption capacity of the CuO-CeO_2 is much stronger than that of the single-component CeO_2 and CuO samples, but also the strong chemisorption peak (283 °C) of CuO-CeO_2 shifts towards a low temperature with increased adsorption, which can be attributed to the synergistic interaction between copper and cerium, related to the formation of Cu–O-Ce solid solution [29,35]. More importantly, the adsorbed ammonia species on the catalyst surface desorb as N_2 and NO_x during the heating cycle, indicating that chemisorbed and lattice oxygen is involved in NH_3 oxidation, while the amount of desorbed N_2 and NO_x reveals the quantity of the active oxygen participating in NH_3 oxidation on the catalyst surface.

Combined with the characterization results, the Cu species primarily existed as Cu–O-Ce solid solutions, and highly dispersed CuO clusters provide sufficient Cu sites and abundant active lattice oxygen for the adsorption and oxidation of NH_3. Since the whole reaction process of NH_3-TPD-MS lacked gas-phase oxygen, the oxygen atoms can only come from chemisorbed, lattice, and internal bulk-phase lattice oxygen on the catalyst. These results cement the role of M−K and L-H mechanisms in the NH_3 catalytic combustion process.

3.3. High concentration NH_3 activity test using different catalysts

The catalytic performance of CuO-CeO_2, CuO and CeO_2 as a function of temperature are evaluated in the high concentration of NH_3 and the results are given in Fig. 3 showing the NH_3 conversion and N_2 selectivity of three catalysts under heating and cooling feeding conditions. The N_2 selectivity is the proportion of product N_2 to the total gas product (after water removal). Under heated feed conditions, the catalytic combustion of NH_3 undergo three sig-

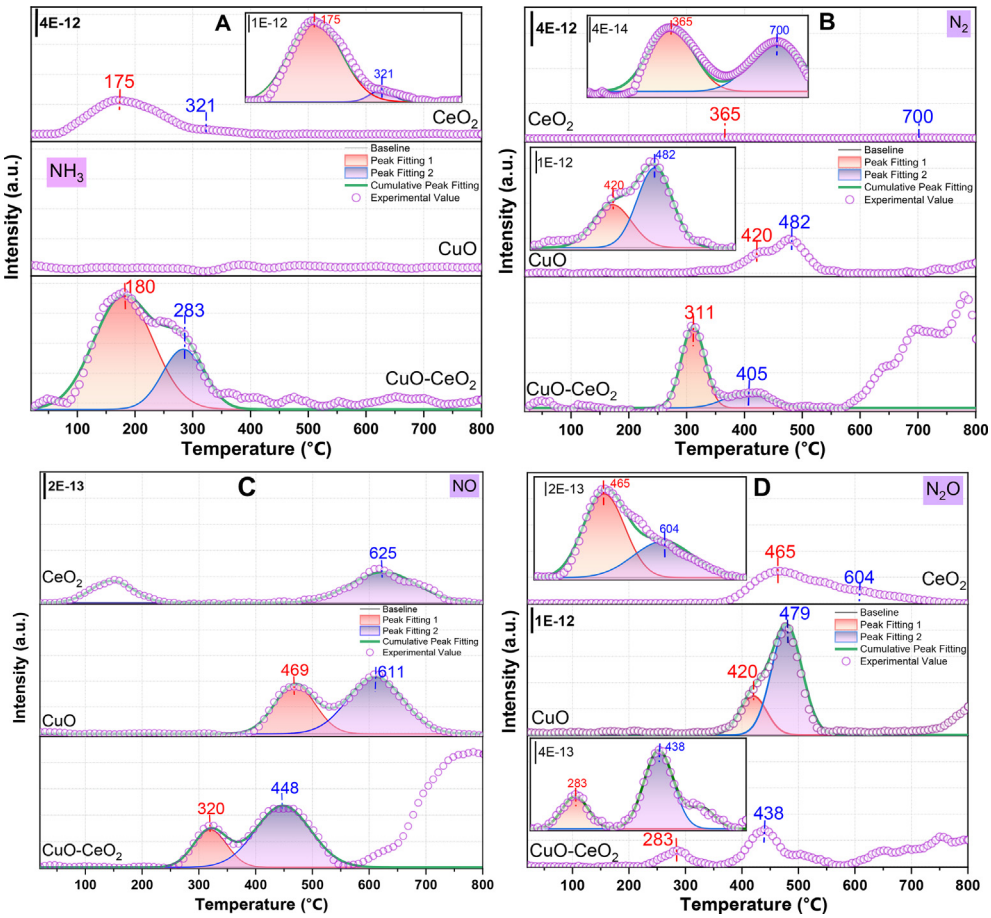

Fig. 2. NH_3-TPD-MS profiles of the CuO, CeO_2, CuO-CeO_2 catalysts. (A) NH_3, (B) N_2, (C) NO, and (D) N_2O. Experimental procedure: no gas-phase oxygen was fed in the experiment; Pretreatment: 100% Ar, 300 °C, 30 min, cooling to 20 °C, ammonia adsorption at 20 °C for 30 min (5% NH_3/Ar) followed by purging with Ar, measurement: 100% Ar, heating rate 10 °C/min from 20 to 800 °C); Flow: 50 ml/min.

nificant steps, i.e., a slow induction process, the catalytic light-off processes, and continuous intense burning. In the presence of 2.5% NH_3 (Fig. 3A), the CuO-CeO_2 catalyst, the NH_3 conversion starts at about 179 °C and continuously increases up to 306 °C until the conversion rate of NH_3 was stable at 91% in the reaction stream and can reach up to 92.7% with subsequently increasing temperature. The reaction is kinetically controlled during the induction phase that occurs at the temperature interval of 179–226 °C (NH_3 conversion < 15%) [36], as reflected in the catalyst bed temperature close to the control temperature. The second step is the transient process of catalytic ignition (226 to 307 °C, 15%<NH_3 conversion < 50%), where the internal diffusion of the catalyst material controlled the reaction rate. This process occurs at the gas–solid phase interface and is probably related to oxygen mobility [16], where the light-off temperature is defined as the temperature (T_{lo}), causing 50% NH_3 conversion. The third phase involves temperatures well above the light-off region. The rapidly increasing temperature translated into the decomposition of adjacent NH_3 and O_2 molecules on the catalyst, which further induced a thermochemical runaway and rapid transition to sustained intense combustion (NH_3 conversion = 50% to 93%). Entering the process into the third stage demonstrated that the reaction rate is dominated by external diffusion.

As shown in Fig. 3 and **Table S1 in Supplementary Note 2**, there is a negligible correlation between T_i and NH_3 concentration. Herein, the temperature corresponding to the induction phase where catalytic combustion of NH_3 just starts to occur is defined as T_i. The CuO-CeO_2 starts to ignite at T_i = 200 °C, while a slight backward temperature shift (20–50 °C) in the induction process for CuO can be found. For CeO_2, it is essentially inactive until 250 °C and starts to exhibit activity only at 300 °C. Therefore, the activities decrease follows the CuO-CeO_2 > CuO > CeO_2 order. Moreover, the corresponding temperatures where the initial maximum NH_3 conversion is reached were similar for the same catalyst. These results demonstrate a synergistic interaction between the Cu and Ce components, rapid change of chemical states in the near-surface region (Cu^+/Cu^{2+} and Ce^{3+}/Ce^{4+}), and strong electronic state interactions [17,32], which significantly enhances the adsorption and activation of NH_3 molecules, which is per H_2-TPR results. Unexpectedly, the N_2 selectivity of the three catalysts appears to decrease at different degrees with increasing temperature. In contrast, the N_2 selectivity of 14% NH_3 (Fig. 3D) do not decrease for the three catalysts and is maintained at 94%~97%. It is thus speculated that in the presence of excess oxygen, NH_x species are partly bound by reactive oxygen with the increase of temperature and partly rapidly oxidized to nitrate species by gas-phase oxygen, and the lack of NH_x hinder the proceeding of i-SCR reaction [17]. In the denitrification experiments (21% O_2, oxygen-enriched state), the NO concentration is found to gradually decrease with increasing temperature (<300 °C), with a maximum NO conversion of 91%, indicating that NO and NH_3 species reacted readily and are effectively removed at low temperatures. At temperatures above 300 °C, the NH_x species react preferentially with O_2 and generated a large amount of NO (**Fig. S3 in Supplementary Note 2**). However, as the amount of NH_x species increase, this situation can most likely be broken and facilitate the i-SCR reaction

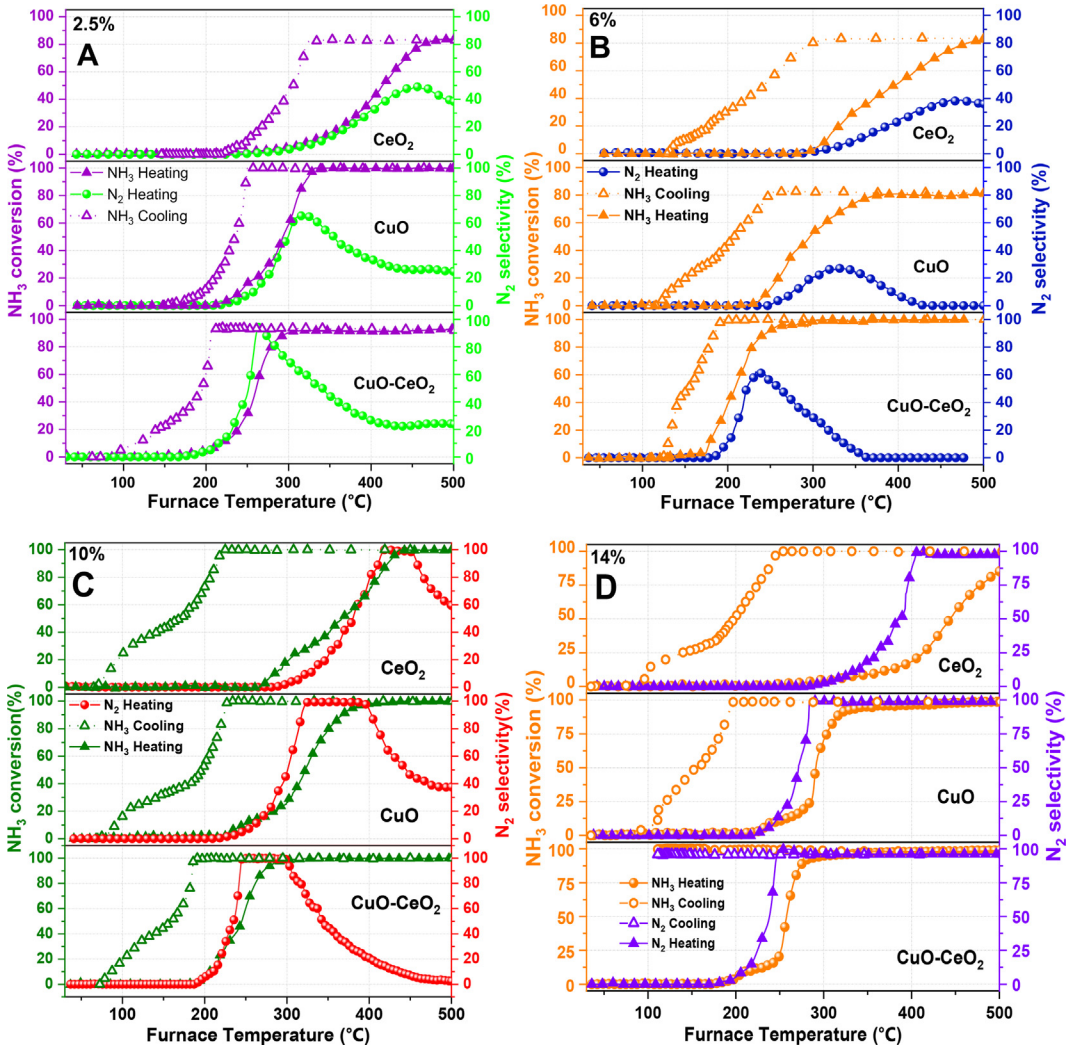

Fig. 3. Catalytic activities of CuO-CeO_2, CuO and CeO_2 at different ammonia concentration, NH_3 concentration of 2.5% (A); 6% (B); 10% (C) and 14% (D); O_2 concentration of 21% and Ar as balance.

path. Thus, an increase in the NH_3/O_2 ratio up to 14%/21% resulted in an increased NH_x species, which leads to the reaction of NO_x +-NH_x to produce N_2 (i-SCR reaction), maintaining a high N_2 selectivity [17,29,37,38]. In contrast, as the NH_3/O_2 ratio decreases with increasing NH_3 concentration, the combination of O and H atoms is more likely to produce H_2O in a state of relative oxygen deficiency.

After cooling the feed, the experiment follows a reverse transition from step 3 to step 1. The extinction temperature (T_{ex}) is defined as the temperature at which 50% NH_3 conversion is achieved under cooled feeding conditions, and the temperature interval corresponds to $\Delta T = T_{lo} - T_{ex}$. In addition, the maximum NH_3 conversion (C_m) and maximum N_2 selectivity (S_m) are also listed in **Table S1 in Supplementary Note 2**. Interestingly, the cooling line for NH_3 conversion shifts to lower temperatures than the heating line (ΔT = 55–245 °C). This hysteresis can result from local heating induced by the exothermic effect of the oxidation reaction or due to the formation or destruction of the active site resulting in an intrinsic change in the catalysts [39]. Moreover, significant broadening of hysteresis can be observed for the CuO and CeO_2 catalysts, with the NH_3 concentration increasing from 2.5% to 14%, corresponding to the ΔT increasing from 57 to 134 °C and 109 to 245 °C, respectively. Notably, when the NH_3 concentration

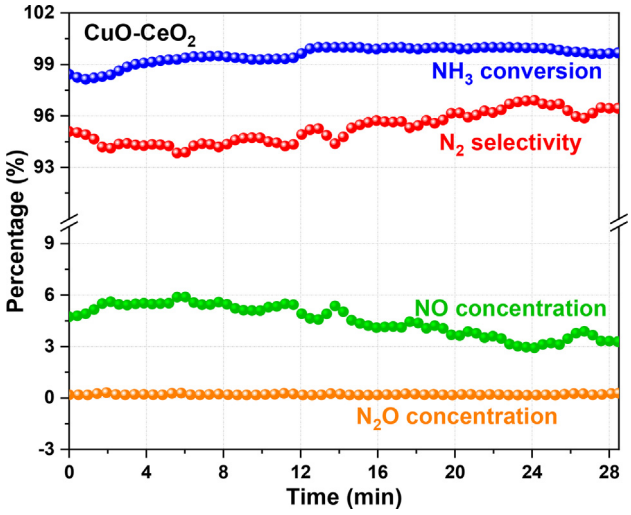

Fig. 4. Percentage content of NO and N_2O, the N_2 selectivity and NH_3 conversion in the self-sustained combustion stage.

increased to 14%, the NH_3 conversion and N_2 selectivity can be continuously maintained even after the heating is stopped for 28 min without deactivation, as shown in Fig. 4. This process is accompanied by the production of a significant amount of NO and a small percentage of N_2O, demonstrating that the rapid mass and heat transfer at the gas–solid phase interface facilitated the self-sustained combustion. A large amount of NO and unreacted NH_3 will be subsequently considered for secondary catalytic combustion to achieve effective removal.

3.4. Analysis of reaction pathways

3.4.1. Kinetic model of NH_3 catalytic ignition

The activity test results reveal the induced ignition process of the CuO-CeO_2 catalyst at around 200 °C. Hence, the kinetic analysis of the induction phase of low NH_3 concentration below 200 °C is carried out to elucidate the predominant reaction mechanism in this stage. Moreover, the heat release of NH_3 catalytic oxidation is up to 906 kJ/mol, where three times the weight of quartz sand is evenly mixed with the catalyst for heat dissipation to exclude the catalyst deactivation possibility. To determine whether the NH_3 reaction is controlled by kinetics, the influence of internal and external diffusion on the reaction rate is excluded under the condition of 15% of the conversion rate of NH_3 **(Supplementary Note 3)** [40].

The kinetics is employed as the primary method to elucidate further the catalytic reaction employing partial pressure of NH_3 and O_2 from 0.1013 to 1.013 kPa and 0.304 to 3.039 kPa **(Table S2 in Supplementary Note 3)**, respectively. The fitting and analysis of the kinetic data results of the NH_3 catalytic oxidation reaction process (Fig. 5) reveal a high fitting accuracy (>0.95), which can be used to establish the kinetic model further. Based on Polymath software, the kinetic model of CuO-CeO_2 is established as follows:

$$r = 5.69 \times 10^{-4} \times Pn^{1.19} Po^{-0.58} \quad (1)$$

The correlation coefficient between the calculated and the experimental results is 0.95. During the NH_3-catalyzed oxidation, the partial pressure of NH_3 significantly affects the NH_3 conversion over CuO-CeO_2. The rate expression exponents of CuO-CeO_2 to NH_3 can reach 1.19, while the rate expression index to O_2 is only −0.58, indicating that the catalytic oxidation reaction of NH_3 mainly depends on the adsorption of NH_3. Moreover, molecular oxygen is adsorbed and disassociated on the catalyst surface, revealing that both molecular adsorbed oxygen (O_2) and atomic adsorbed oxygen (O) existed on the catalyst surface, which is confirmed by isotope ($^{18}O_2$) experiments. Meanwhile, it provides the possibility of the existence of the L-H mechanism. According to the Arrhenius equation, the activation energy of CuO-CeO_2 can be calculated as 97 kJ/mol.

The formation of Cu–O-Ce solid solution in CuO-CeO_2 catalyst plays a vital role in the catalytic oxidation of NH_3. It has been widely demonstrated that the lattice oxygen provided by Cu–O-Ce solid solution can react with the active intermediate NH_x to form N_2 and N_2O [16,20]. Moreover, the presence of Cu–O-Ce solid solution can promote the activation of gas-phase oxygen and the formation and migration of lattice oxygen in the NH_3-catalyzed combustion reaction [16]. Consequently, combining the kinetic and NH_3-TPD-MS experimental results, the lattice oxygen (i.e., the M−K mechanism) also occupy a relatively important position in the low-temperature induction stage, which will be discussed in the next isotope ($^{18}O_2$)-transient response experiments (low-temperature induction process).

From activity experiments, the data of NH_3 and N_2 heating lines overlap at<15% NH_3 conversion, demonstrating NH_3 is converted entirely to N_2 in the induction phase with little NO_x generation, which can be attributed to the low rate of NH_3 oxidation at a lower temperature, resulting in the rapidly released heat which is difficult to accumulate. In turn, the reaction path of N_2 generation is more likely to occur at the low reaction temperature. For CuO-CeO_2, the 15% NH_3 conversion corresponds to temperatures already in the range of 220 to 240 °C. However, Sun et al. [22] found that the L-H mechanism predominantly occurs below 200 °C; hence, the L-H mechanism may be observed below 200 °C, i.e., at lower NH_3 conversion rate, which will be discussed in transient response experiments in the induction phase (200 °C). At a high temperature, the NO_x generation increases significantly after entering a continuous and intense combustion phase, illustrating a change in the reaction pathway or a variation in the ratio of the different reaction pathways. Similarly, a decrease in NO_x

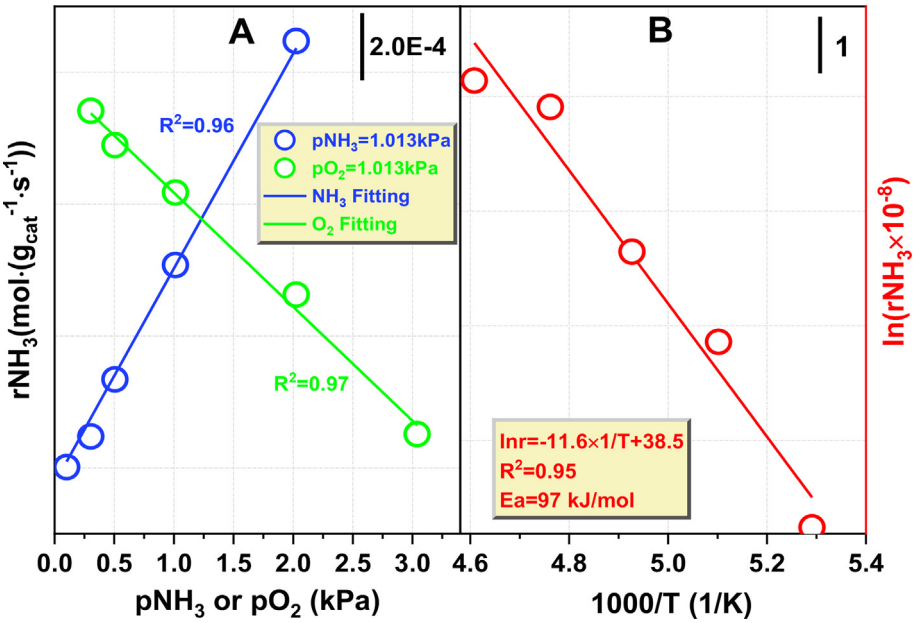

Fig. 5. Kinetic results over the CuO-CeO_2 catalyst (A) and activation energy for the NH_3 oxidation reaction over the catalyst (B).

generation with increased NH_3 concentration (as reflected in the active experiment) suggests that increased NH_3 species promote the i-SCR reaction.

3.4.2. Transient response experiments

To identify the mechanisms more clearly in the low-temperature induction stage and high-temperature continuous combustion stage, transient response experiments are employed (Fig. 6). After 30 min of NH_3 adsorption saturation, 5% NH_3/Ar (100 ml/min) is removed from the feed stream while the catalyst is continuously flushed with argon until stable baseline. The 8% O_2/Ar is instantaneously fed at 410 s, and the adsorbed NH_3 species are gradually oxidized by reactive oxygen species to produce N_2, H_2O, and a small amount of NO_x, considering the continued heat accumulation that cannot be released in time and the process is accompanied by the desorption of NH_3. It is implied that the gas-phase oxygen can adsorb on the catalyst surface, accelerating the adsorption rate since NH_3 adsorption on the catalyst surface is dominated, and such a surface steady state prevents the adsorption and dissociation of gaseous O_2 from being broken gradually. The NH_3 species can be oxidized by adsorbed oxygen to liberate N_2 and NO_x, suggesting the dominance of L-H mechanisms under the low-temperature induction stage.

Based on the above characterization results, it is evident that the addition of copper changes the original crystal structure of CeO_2, which can promote the oxygen transfer ability of CeO_2 and form Cu^+-[O_v]-Ce^{3+} ([O_v] = surface oxygen vacancy) at the Cu-Ce interface, suggesting a large amount of lattice oxygen at the Cu-Ce interface, which is further confirmed by the transient response experiment (high-temperature continuous combustion stage) of the CuO-CeO_2 catalyst (Fig. 6B). The CuO-CeO_2 sample (200 mg) is pretreated with Ar gas purgatory at 300 ℃ for 30 min. In the first stage, a mixture of 5% NH_3 + 8% O_2/Ar is purged into the tubular furnace reactor, followed by O_2, N_2, and N_2O signals exhibiting a sharp step response. The N_2 quickly responded and is produced initially. The NO production rate is significantly lower than N_2O, indicating that the reaction barrier for N_2O is notably lower than for NO at 300 °C from 50 to 61 s. However, the concentration of NO is higher than N_2O after reaching equilibrium at 125 s, which is also confirmed in NH_3-TPD experiments. Moreover, the NH_3 signal gradually increases and stabilizes at 127 s, proving that some NH_3 is still not involved in the reaction and escaped directly under such conditions. Subsequently, the Ar is purged in the second stage until all detected gas signals get zero. Meanwhile, the N_2, O_2, and N_2O signals quickly drop to baseline during this stage, while the NH_3, H_2O, and NO signals are not dropped to baseline until 175 s, implying that in the absence of NH_3 and O_2, the adsorbed nitrate continues to decompose under conditions of reduced gas-phase NO_x, and N_2 partial pressures. It is worth mentioning that during the third stage (part (c)), adding 5% NH_3/Ar rapidly increased N_2 signal intensity, which is 3.38% (absolute difference) higher than the maximum value observed in the first stage (part (a)). Furthermore, even after smoothing the curve, the electrical signal remains more considerable than observed in the first stage, indicating competitive adsorption between NH_3 and O_2 in the first stage. The reaction of adsorbed NH_3 and O_2 implies the existence of the L-H mechanism; nevertheless, adsorbed NH_3 and lattice oxygen follows the M−K mechanism. Meanwhile, the signal intensity of NO and N_2O is significantly lower than that of the first stage, and the signal intensity of NH_3 is stable at the baseline, indicating that the conversion rate of NH_3 reached nearly 100%, with no NH_3 escape. After 237 s, the N_2 signal starts to decrease until reaching the baseline since the lattice oxygen in the catalyst is entirely consumed. It means that in the absence of gas-phase oxygen, the conversion of NH_3 is higher with superior N_2 selectivity when a large amount of lattice oxygen is involved in the reaction.

3.4.3. Isotope ($^{18}O_2$)-transient response experiments

The isotope ($^{18}O_2$)-transient response experiments provide an insight into the contribution of the L-H (^{18}O, contribution of adsorbed oxygen) and the M−K mechanism (^{16}O, contribution of lattice oxygen) in both stages (Fig. 7). From the isotope ($^{18}O_2$)-transient response experiment in the induction (200 °C) and sustained combustion phase (300 °C), the presence of $^{16}O^{18}O$ suggests that some of the gas-phase $^{18}O_2$ dissociates upon adsorption on the catalyst surface to form ^{18}O atoms and is displaced with lattice oxygen (^{16}O) to form $^{16}O^{18}O$. The $H_2^{18}O$ and $H_2^{16}O$, $N^{18}O$ and $N^{16}O$, $N_2^{16}O$ and $N_2^{18}O$ as the products are detected, implying that the adsorbed ($^{18}O_2$, $^{18}O^-$) and lattice oxygen ($^{16}O^{2-}$) are involved in the reaction, confirming the coexistence of the L-H and M−K mechanisms. These results are also demonstrated in the NH_3-TPD experiment since the whole reaction process of NH_3-TPD runs lacked gas-phase oxygen, and the oxygen atoms can only come from chemisorbed, lattice, and internal bulk-phase lattice oxygen on the catalyst surface.

As the ^{18}O and ^{16}O involved in the reaction eventually enter into H_2O, NO and N_2O (conservation of oxygen element), the area integral of the electric signal curves of each gas can be obtained, i.e., in the induction stage (S1/S2 = 0.427), and in the continuous combustion stage (S1/S2 = 0.627, S1 is the relative content of ^{16}O, S2 is the relative content of ^{18}O). The L-H mechanism (^{18}O, contribution of adsorbed oxygen) plays a dominant role in the induction stage, while the M−K mechanism (^{16}O, contribution of lattice oxygen) significantly increases in the sustained combustion stage.

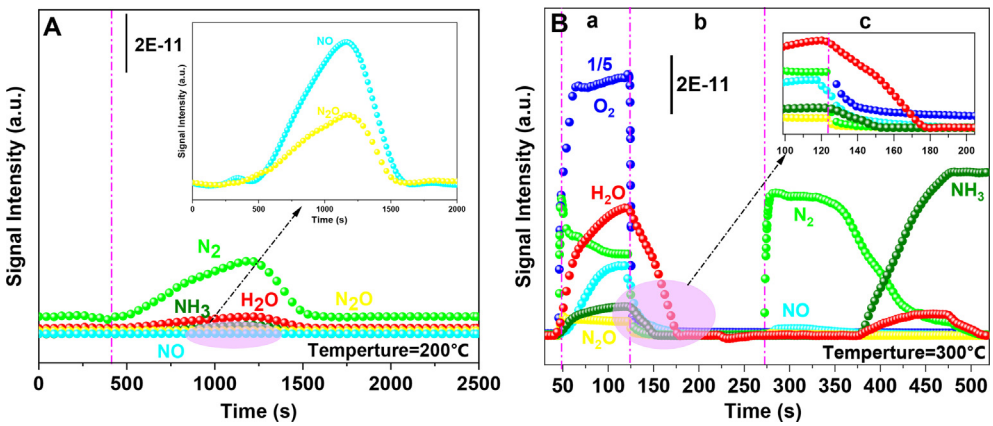

Fig. 6. Transient experimental results of CuO-CeO_2 catalyst. (A) The slow induction stage (B) the sustained combustion stage.

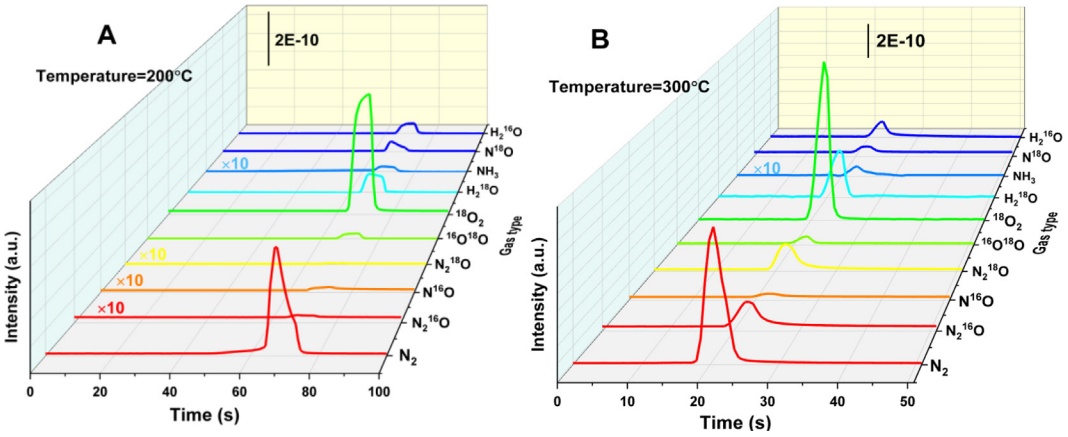

Fig. 7. Isotope ($^{18}O_2$) - transient response experiments. (A) the induction stage (B) the sustained combustion stage. Experimental procedure: 1) pretreatment with Ar by heating to 300 °C for 30 min and then cooling to room temperature; 2) pass 5% NH_3/Ar and adsorb at room temperature for 30 min, 3) purge with Ar to 200 °C (the induction stage) or 300 °C (the sustained combustion stage) at 10 °C/min and keep the temperature constant until the baseline is smooth; 4) instantly pass 10 ml $^{18}O_2$/Ar and observe the gas signal change.

3.5. Analysis of reaction paths using FT-IR

The IR technique elucidate the formation and conversion of intermediates and the detailed reaction process in two stages (induction and continuous combustion stage) and to understand why the high NH_3 concentration possessed a high N_2 selectivity. Briefly, the IR chamber is purged with Ar and heated to 300 °C to remove the impurities in the chamber and adsorbed on the catalyst, creating a homogenous environment. Subsequently, 5% NH_3 + 8% O_2/Ar is fed into the cell, and the temperature is increased to 500 °C at the rate of 10 °C/min.

The IR results on CuO-CeO_2 and CeO_2 catalysts are shown in Fig. 8. The peak at 1621 cm^{-1} is attributed to asymmetric deformation of NH_3 molecules coordinated on the Lewis acid site [17,41], and the band at 1714 cm^{-1} exhibited the characteristics of the Brønsted acid site (NH_4^+) [41–43]. Several spectral bands in the range of 3500 ∼ 3200 cm^{-1} can be ascribed to the N–H stretching vibration modes in coordinated NH_3 [28]. In addition, the band at 1534 cm^{-1} is assigned to nitrosyl (–HNO) species [17]. For the CuO-CeO_2 and CeO_2, the HNO (1534 cm^{-1}), NH_2 (1621 cm^{-1}), and NH (3200 ∼ 3500 cm^{-1}) moieties appear to be the bands starting from 30 °C, where the peak intensity increases gradually with increasing temperature (<270 °C), indicating that upon heating, the reactions of dehydrogenation and oxidation have proceeded as follows:

$$NH_3(g) \rightarrow NH_3(ad) \rightarrow NH_2(ad) + H$$
$$NH_3(g) \rightarrow NH_4^+(ad) \rightarrow NH_2(ad) + 2H \quad (1)$$

$$NH_2(ad) \rightarrow NH(ad) + H \quad (2)$$

Combining kinetic and transient response experimental results, the activated oxygen (O) is primarily derived from adsorbed and lattice oxygen and bounded to low-temperature NH_x species [41]. The accumulation of large amounts of –HNO resulted in the generation of N_2 and NO_x, while N_2O is to be generated before NO formation, as shown in equation reaction (3) ∼ (6). This is in agreement with the activation energy of generation calculated with the Freeman-Carroll equation and the transient response experiment. From reaction (5), it is clear that NH is the key species for forming N_2 in the low temperature steady state stage, and the presence of nitrite (–HNO) facilitated the SCR reaction at low temperatures.

$$NH(ad) + O \rightarrow HNO(ad) \quad (3)$$

$$HNO(ad) + HNO(ad) \rightarrow N_2O + H_2O \quad (4)$$

$$HNO(ad) + NH(ad) \rightarrow N_2 + H_2O \quad (5)$$

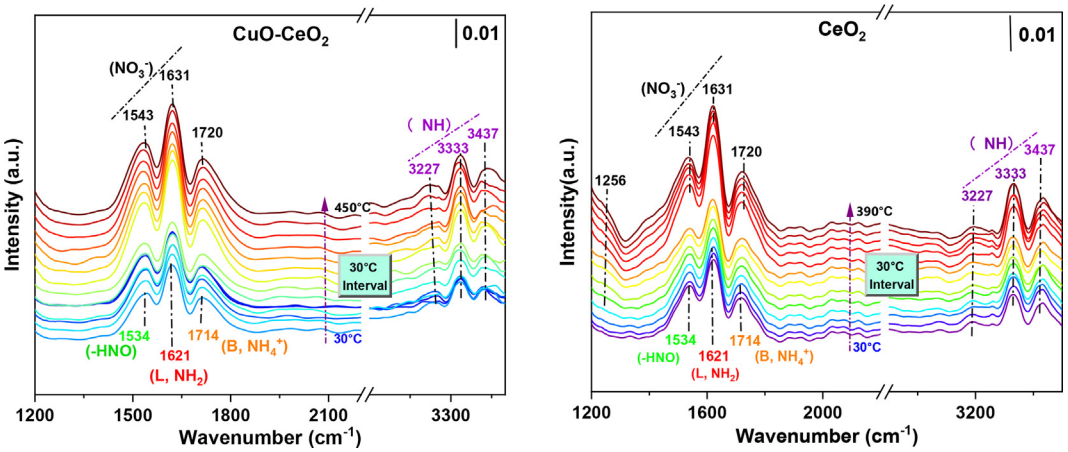

Fig. 8. In situ infrared spectroscopy analysis of CuO-CeO_2 and CeO_2. Pretreatment: 100% Ar at 300 °C for 30 min; Measurement conditions: 5% NH_3 + 8%O_2/Ar (200 ml/min), heating up to 500 °C (10 °C/min).

$$HNO(ad) + O \rightarrow NO + OH \quad (6)$$

For CuO-CeO_2 and CeO_2, the bands at 1543 cm^{-1} and 1631 cm^{-1} are principally attributed to monodentate nitrate and bridged nitrate, respectively [17,28], which accumulated with increasing temperature (>270 °C, reaction (7) ~ (9)). For CeO_2, a more obvious band appeared at 1270 cm^{-1}, ascribed to the bidentate nitrate [28]. The strength of multiple bands is significantly enhanced at temperatures higher than 270 °C, implying that the adsorption of NH_3, dehydrogenation, and nitrate species is in a new dynamic equilibrium state. Dehydrogenation and oxidation co-occurred in this process and the new nitrate species were produced along with the NH_3 species. Therefore, peaks' formation and disappearance were challenging to apprehend directly.

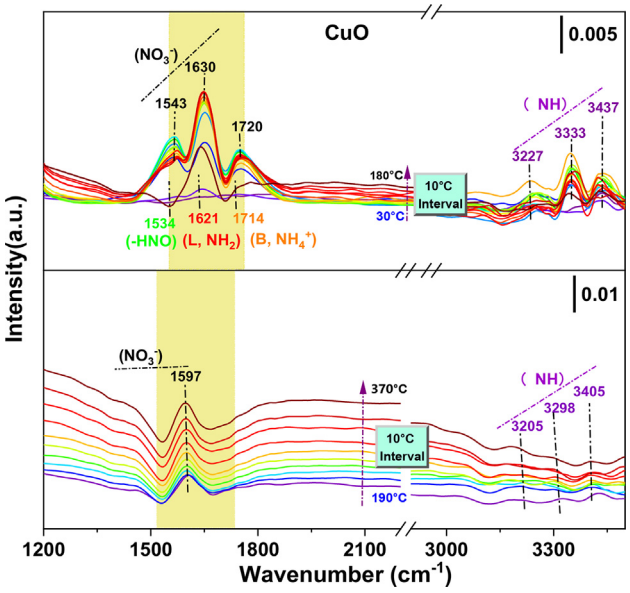

Fig. 9. In situ infrared spectroscopy analysis of CuO. Pretreatment: 100% Ar at 300 °C for 30 min; Measurement conditions: 5% NH_3 + 8%O_2/Ar (200 ml/min), heating up to 500 °C (10 °C/min).

$$NH(ad) + O \rightarrow NO_3^-(monodentate\ or\ bidentate\ nitrate) + OH \quad (7)$$

$$NH(ad) + NO_3^-(monodentate\ \text{or}\ bidentate\ nitrate) \rightarrow N_2O + H \quad (8)$$

$$NH_2(ad) + NO_3^-(monodentate\ \text{or}\ bidentate\ nitrate) \rightarrow N_2 + H_2O\ (i-SCR) \quad (9)$$

The NH_3 is oxidized following dehydrogenation to produce NO, while the NH_2 species, an important intermediate in SCR reactions, can react with NO to produce N_2 and H_2O (reaction (10) [44,45], demonstrating that NH_2 is the key species for the generation of N_2. Combined with the activity experiments, reactions (9) to (10) are the dominant steps in the high-temperature continuous combustion stage, enabling three catalysts to maintain high N_2 selectivity at 14% NH_3 concentration.

$$NH_2(ad) + NO \rightarrow N_2 + H_2O(i-SCR) \quad (10)$$

The IR spectral result of CuO is shown in Fig. 9, which is significantly differentiated from the IR spectra of CuO-CeO_2 and CeO_2. The band at HNO (1534 cm^{-1}) and NH (3200 ~ 3500 cm^{-1}) moieties appear at 30 °C and nearly disappear at 180 °C. The 1621 cm^{-1} appears from 60 °C, decreases abruptly at 180 °C, subsequently disappears at 190 °C. Meanwhile, a new peak is generated for bidentate nitrate (1597 cm^{-1}). The NH_3 adsorbed on the Lewis acid sites is converted to NH_x by dehydrogenation, and the elevated temperature-induced oxidation of NH_x to bidentate nitrate (bi-NO_x, reaction (11)~(12)). The accumulation of bidentate nitrates and the disappearance of intermediate substances allow NH_3 catalytic combustion reaction to proceed continuously (a new dynamic equilibrium).

$$NH(ad) + NO_3^-(bidentate\ nitrate) \rightarrow N_2O + H \quad (11)$$

$$NH_2(ad) + NO_3^-(bidentate\ nitrate) \rightarrow N_2 + H_2O\ (i-SCR) \quad (12)$$

In conclusion, the gaseous molecule NH_3(g) can first form adsorbed NH_3(ad) at the catalyst's Lewis acid and Brønsted acid sites. The dehydrogenation of NH_3 occurs almost simultaneously, and NH_3(ad) or NH_4^+ binds the catalyst oxygen to form NH_x, and OH intermediates [46]. These results suggest that with the increase

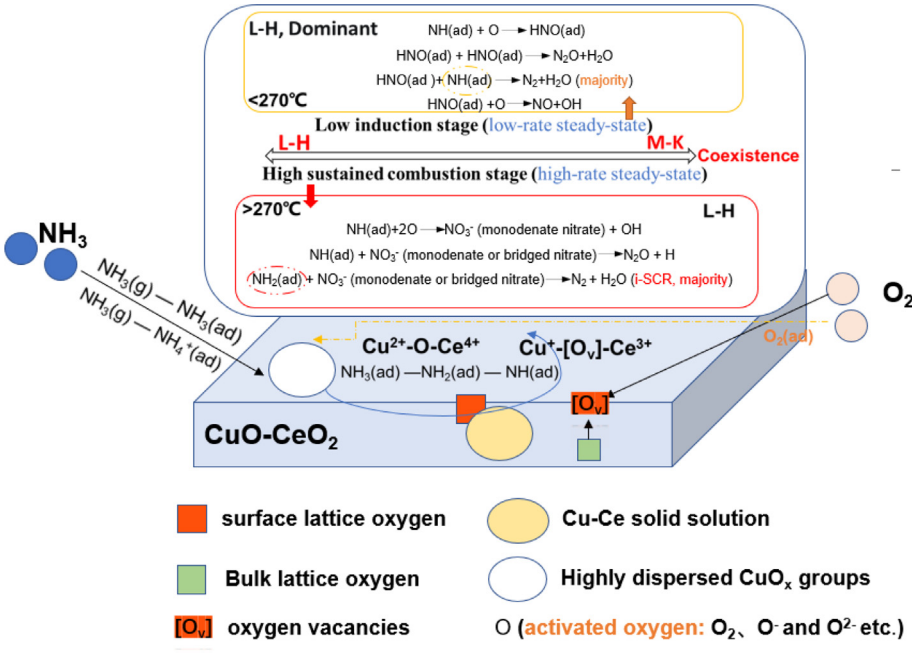

Scheme 1. Reaction pathways and mechanisms for CuO-CeO_2 catalyst.

in sample temperature, the adsorption of NH_3 components and atomic oxygen rapidly desorb and reacts to form nitrosyl (–HNO) species. Moreover, the presence of nitrite is beneficial for SCR reaction at low temperatures [45], which demonstrated that most of the N_2 should come from the i-SCR reaction of different nitrates, NO combined with NH_2 at high-temperature steady state, which can explain the activity results (high N_2 selectivity in the high temperature sustained combustion stage). In the NH_3 catalytic combustion reaction, different types of oxygen species are involved in the reaction, and increasing the amount of NH_x facilitated the i-SCR, which can improve the N_2 selectivity. The overall concept diagram is as follows (Scheme 1).

4. Conclusions

The self-sustained catalytic combustion mode for high NH_3 concentration is researched by CuO, CeO_2, and CuO-CeO_2 catalysts to systematically reveal the mechanisms at the induction and sustained combustion stages. In the catalytic combustion of NH_3 at high concentrations, the activity of catalysts followed the order of CuO-CeO_2 > CuO > CeO_2. The XRD, Raman, and XPS characterization results demonstrate that adding Cu resulted in the formation of finely dispersed CuO_x clusters on CeO_2, inducing CeO_2 lattice distortion and generating more oxygen vacancies. There are enough Cu sites on the CuO-CeO_2 catalyst surface to adsorb NH_3 and abundant active lattice oxygen. The NH_3-TPD results show that the adsorption capacity of the CuO-CeO_2 is significantly higher than single-component CeO_2 and CuO samples, which is attributable to the synergistic interaction between copper and cerium, related to the formation of Cu–O-Ce solid solution.

The criterion for self-sustaining catalytic combustion relies on enough heat release to maintain the reaction temperature at the catalyst bed, allowing the reaction to proceed continuously. The CuO-CeO_2 can achieve self-sustained catalytic combustion with a 14% concentration of NH_3, exhibiting 94%∼97% N_2 selectivity. In this process, the lattice oxygen (O_{lat}) escapes from the Cu cation, migrating to the surface, followed by a reaction with the formed NH_3 species due to the concentration gradient. Adding Cu ensured its existence in highly dispersed CuO and Cu–O-Ce solid solutions and provided sufficient Cu sites for the adsorption of NH_3 and active lattice oxygen.

Catalytic ignition triggered a kinetic transition from low-rate to high-rate steady-state. According to isotope ($^{18}O_2$)-transient experiments, three types of oxygen are involved in the catalytic combustion of NH_3, i.e., adsorbed molecular (O_2), atomic adsorbed (O^-), and lattice oxygen (O^{2-}). The L-H mechanism (^{18}O, contribution of adsorbed oxygen) plays a relatively dominant role in the induction stage (S1 is the relative content of ^{16}O, and S2 is the relative content of ^{18}O). The contribution of the M−K mechanism (^{16}O, contribution of lattice oxygen), corresponding to S1/S2 = 0.627, is significantly increased in the sustained combustion stage. The IR results indicate that NH and NH_2 are separately key species for the two stages of N_2 production (i-SCR). Meanwhile, most of the N_2 should come from the i-SCR reaction of different nitrates, NO combined with NH_2 at a high-temperature steady state, resulting in a high N_2 selectivity when the N_2 concentration reaches 14%.

Data availability

Data will be made available on request.

Declaration of Competing Interest

The authors declare that they have no known competing financial interests or personal relationships that could have appeared to influence the work reported in this paper.

Acknowledgments

We gratefully acknowledge the financial support from the National Natural Science Foundation of China (No. 52176142).

Appendix A. Supplementary material

Supplementary data to this article can be found online at https://doi.org/10.1016/j.jcat.2023.06.006.

References

[1] Q. Zhang, L. Guo, X. Cai, S. Shan, K. Li, J. Zhao, Z. Zhou, Chemical effect of CH_4 on NH_3 combustion in an O_2/N_2 environment via ReaxFF, Energy Fuel 35 (2021) 10918–10928.
[2] C. Filipe Ramos, R.C. Rocha, P.M.R. Oliveira, M. Costa, X.-S. Bai, Experimental and kinetic modelling investigation on NO, CO and NH_3 emissions from NH_3/CH_4/air premixed flames, Fuel 254 (2019).
[3] H. Shi, S. Liu, C. Zou, L. Dai, J. Li, W. Xia, J. Yang, J. Luo, W. Li, Experimental study and mechanism analysis of the NO_x emissions in the NH_3 MILD combustion by a novel burner, Fuel 310 (2022).
[4] Z. Wang, X. Han, Y. He, R. Zhu, Y. Zhu, Z. Zhou, K. Cen, Experimental and kinetic study on the laminar burning velocities of NH_3 mixing with CH_3OH and C_2H_5OH in premixed flames, Combust. Flame 229 (2021).
[5] G.B. Ariemma, G. Sorrentino, R. Ragucci, M. de Joannon, P. Sabia, Ammonia/Methane combustion: Stability and NO_x emissions, Combust. Flame 241 (2022).
[6] G.J. Kim, D.W. Kwon, J.H. Shin, K.W. Kim, S.C. Hong, Influence of the addition of vanadium to Pt/TiO_2 catalyst on the selective catalytic oxidation of NH_3 to N_2, Environ. Technol. 40 (2019) 2588–2600.
[7] M. Sun, S. Wang, Y. Li, H. Xu, Y. Chen, Promotion of catalytic performance by adding W into Pt/ZrO_2 catalyst for selective catalytic oxidation of ammonia, Appl. Surf. Sci. 402 (2017) 323–329.
[8] Z. Wang, Q. Sun, D. Wang, Z. Hong, Z. Qu, X. Li, Hollow ZSM-5 zeolite encapsulated Ag nanoparticles for SO_2-resistant selective catalytic oxidation of ammonia to nitrogen, Sep. Purif. Technol. 209 (2019) 1016–1026.
[9] G. Qi, J.E. Gatt, R.T. Yang, Selective catalytic oxidation (SCO) of ammonia to nitrogen over Fe-exchanged zeolites prepared by sublimation of $FeCl_3$, J. Catal. 226 (2004) 120–128.
[10] J. Guo, W. Yang, Y. Zhang, L. Gan, C. Fan, J. Chen, Y. Peng, J. Li, A multiple-active-site Cu/SSZ-13 for NH_3-SCO: Influence of Si/Al ratio on the catalytic performance, Catal. Commun. 135 (2020).
[11] R.Q. Long, R.T. Yang, Superior ion-exchanged ZSM-5 catalysts for selective catalytic oxidation of ammonia to nitrogen, Chem. Commun. (2000) 1651–1652.
[12] D. Song, X. Shao, M. Yuan, L. Wang, W. Zhan, Y. Guo, Y. Guo, G. Lu, Selective catalytic oxidation of ammonia over MnO_x–TiO_2 mixed oxides, RSC Adv. 6 (2016) 88117–88125.
[13] H. Wang, Q. Zhang, T. Zhang, J. Wang, G. Wei, M. Liu, P. Ning, Structural tuning and NH_3-SCO performance optimization of CuO-Fe_2O_3 catalysts by impact of thermal treatment, Appl. Surf. Sci. 485 (2019) 81–91.
[14] P. Li, R. Zhang, N. Liu, S. Royer, Efficiency of Cu and Pd substitution in Fe-based perovskites to promote N_2 formation during NH_3 selective catalytic oxidation, NH3-SCO, Appl Catal B 203 (2017) 174–188.
[15] C. Liang, X. Li, Z. Qu, M. Tade, S. Liu, The role of copper species on Cu/γ-Al_2O_3 catalysts for NH_3–SCO reaction, Appl. Surf. Sci. 258 (2012) 3738–3743.
[16] Z. Wang, Z. Qu, X. Quan, Z. Li, H. Wang, R. Fan, Selective catalytic oxidation of ammonia to nitrogen over CuO-CeO_2 mixed oxides prepared by surfactant-templated method, Appl Catal B 134–135 (2013) 153–166.
[17] X. Zhang, H. Wang, Z. Wang, Z. Qu, Adsorption and surface reaction pathway of NH_3 selective catalytic oxidation over different Cu-Ce-Zr catalysts, Appl. Surf. Sci. 447 (2018) 40–48.
[18] R.-M. Yuan, G. Fu, X. Xu, H.-L. Wan, Mechanisms for Selective Catalytic Oxidation of Ammonia over Vanadium Oxides, J. Phys. Chem. C 115 (2011) 21218–21229.
[19] L. Peng, A. Guo, D. Chen, P. Liu, B. Peng, M. Fu, D. Ye, P. Chen, Ammonia Abatement via Selective Oxidation over Electron-Deficient Copper Catalysts, Environ. Sci. Tech. 56 (2022) 14008–14018.
[20] Z. Qu, Z. Wang, X. Zhang, H. Wang, Role of different coordinated Cu and reactive oxygen species on the highly active Cu–Ce–Zr mixed oxides in NH_3-

SCO: a combined in situ EPR and O_2-TPD approach, Catalysis, Sci. Technol. 6 (2016) 4491–4502.
[21] J. Zhou, R.t. Guo, X.-F. Zhang, Y.-Z. Liu, C.-P. Duan, G.-L. Wu, W.J.E. Pan, Fuels,, Cerium Oxide-Based Catalysts for Low-Temperature Selective Catalytic Reduction of NO_x with NH_3, A Review 35 (2021) 2981–2998.
[22] P. Sun, R.-T. Guo, S.-M. Liu, S.-X. Wang, W.-G. Pan, M.-Y. Li, S.-W. Liu, J. Liu, X. Sun, Enhancement of the low-temperature activity of Ce/TiO_2 catalyst by Sm modification for selective catalytic reduction of NO_x with NH_3, Molecular, Catalysis 433 (2017) 224–234.
[23] P. Tunå, J. Brandin, Selective catalytic oxidation of ammonia by nitrogen oxides in a model synthesis gas, Fuel 105 (2013) 331–337.
[24] C. Wang, D. Ren, G. Harle, Q. Qin, L. Guo, T. Zheng, X. Yin, J. Du, Y. Zhao, Ammonia removal in selective catalytic oxidation: Influence of catalyst structure on the nitrogen selectivity, J. Hazard. Mater. 416 (2021).
[25] Z. Wang, Z. Qu, X. Quan, H. Wang, Selective catalytic oxidation of ammonia to nitrogen over ceria–zirconia mixed oxides, Appl. Catal. A 411–412 (2012) 131–138.
[26] C.-M. Hung, Selective Catalytic Oxidation of Ammonia to Nitrogen on CuO-CeO_2 Bimetallic Oxide Catalysts, Aerosol Air Qual. Res. 6 (2006) 150–169.
[27] F. Bin, R. Kang, X. Wei, Q. Hao, B. Dou, Self-sustained combustion of carbon monoxide over $CuCe_{0.75}Zr_{0.25}O_\delta$ catalyst: Stability operation and reaction mechanism, Proceedings of the Combustion Institute, 37 (2019) 5507-5515.
[28] S. Ali, L. Chen, F. Yuan, R. Li, T. Zhang, S.u.H. Bakhtiar, X. Leng, X. Niu, Y. Zhu,, Synergistic effect between copper and cerium on the performance of Cu_x-$Ce_{0.5-x}$-$Zr_{0.5}$ (x=0.1–0.5) oxides catalysts for selective catalytic reduction of NO with ammonia, Appl Catal B 210 (2017) 223–234.
[29] X. Zhang, H. Wang, X. Jiang, H. Sun, Z. Qu, Study of synergistic effect between CuO and CeO_2 over CuO@CeO_2 core–shell nanocomposites for NH_3-SCO, Catalysis, Sci. Technol. 9 (2019) 2968–2981.
[30] P.G. Smirniotis, P.M. Sreekanth, D.A. Peña, R.G. Jenkins, Manganese Oxide Catalysts Supported on TiO_2, Al_2O_3, and SiO_2: A Comparison for Low-Temperature SCR of NO with NH_3, Ind. Eng. Chem. Res. 45 (2006) 6436–6443.
[31] R.Q. Long, R.T. Yang, Selective Catalytic Oxidation of Ammonia to Nitrogen over Fe_2O_3–TiO_2 Prepared with a Sol-Gel Method, J. Catal. 207 (2002) 158–165.
[32] R. Kang, P. Ma, J. He, H. Li, F. Bin, X. Wei, B. Dou, K.N. Hui, K.S. Hui, Transient behavior and reaction mechanism of CO catalytic ignition over a CuO–CeO_2 mixed oxide, Proc. Combust. Inst. 38 (2021) 6493–6501.
[33] Y. Zheng, K. Li, H. Wang, Y. Wang, D. Tian, Y. Wei, X. Zhu, C. Zeng, Y. Luo, Structure dependence and reaction mechanism of CO oxidation: A model study on macroporous CeO_2 and CeO_2-ZrO_2 catalysts, J. Catal. 344 (2016) 365–377.
[34] P.D. Garn, An examination of the kinetic compensation effect, J. Therm. Anal. 7 (1975) 475–478.
[35] Y. Lu, S. Jiang, S. Wang, Y. Zhao, X. Ma, Effect of the addition of Ce and Zr over a flower-like NiO-MgO (111) solid solution for CO_2 reforming of methane, Journal of CO_2 Utilization 26 (2018) 123–132.
[36] H. Wang, Z. Qu, S. Dong, C. Tang, Mechanistic Investigation into the Effect of Sulfuration on the FeW Catalysts for the Selective Catalytic Reduction of NO_x with NH_3, ACS Appl. Mater. Interfaces 9 (2017) 7017–7028.
[37] C. Zheng, H. Zhao, The microscopic oxidation mechanism of NH_3 on CuO(111): A first-principles study, Fuel Process. Technol. 213 (2021).
[38] M. Jabłońska, TPR study and catalytic performance of noble metals modified Al_2O_3, TiO_2 and ZrO_2 for low-temperature NH_3-SCO, Catal. Commun. 70 (2015) 66–71.
[39] W. Gac, The influence of silver on the structural, redox and catalytic properties of the cryptomelane-type manganese oxides in the low-temperature CO oxidation reaction, Appl Catal B 75 (2007) 107–117.
[40] W. Chen, J. Cao, J. Yang, Y. Cao, H. Zhang, Z. Jiang, J. Zhang, G. Qian, X. Zhou, D. Chen, W. Yuan, X. Duan, Molecular-level insights into the electronic effects in platinum-catalyzed carbon monoxide oxidation, Nat. Commun. 12 (2021) 6888.
[41] L. Zhang, H. He, Mechanism of selective catalytic oxidation of ammonia to nitrogen over Ag/Al_2O_3, J. Catal. 268 (2009) 18–25.
[42] F. Bin, C. Song, G. Lv, J. Song, S. Wu, X. Li, Selective catalytic reduction of nitric oxide with ammonia over zirconium-doped copper/ZSM-5 catalysts, Appl Catal B 150–151 (2014) 532–543.
[43] M.A. Larrubia, G. Ramis, G. Busca, An FT-IR study of the adsorption and oxidation of N-containing compounds over Fe_2O_3-TiO_2 SCR catalysts, Appl Catal B 30 (2001) 101–110.
[44] X. Yao, L. Chen, J. Cao, Y. Chen, M. Tian, F. Yang, J. Sun, C. Tang, L. Dong, Enhancing the deNO_x performance of MnOx/CeO_2-ZrO_2 nanorod catalyst for low-temperature NH_3-SCR by TiO_2 modification, Chem. Eng. J. 369 (2019) 46–56.
[45] G. Yang, H. Zhao, X. Luo, K. Shi, H. Zhao, W. Wang, Q. Chen, H. Fan, T. Wu, Promotion effect and mechanism of the addition of Mo on the enhanced low temperature SCR of NO_x by NH_3 over $MnO_{x/\gamma}$-Al_2O_3 catalysts, Appl Catal B 245 (2019) 743–752.
[46] W. Chen, Y. Ma, Z. Qu, Q. Liu, W. Huang, X. Hu, N. Yan, Mechanism of the selective catalytic oxidation of slip ammonia over Ru-modified Ce-Zr complexes determined by in situ diffuse reflectance infrared Fourier transform spectroscopy, Environ. Sci. Tech. 48 (2014) 12199–12205.